
Tera-MIND: Tera-scale mouse brain simulation via spatial mRNA-guided diffusion

Jiqing Wu¹, Ingrid Berg², Yawei Li^{3,4}, Ender Konukoglu³, Viktor H. Koelzer^{1,5,*}

¹Department of Biomedical Engineering, University of Basel, Switzerland.

²Department of Pathology and Molecular Pathology, University Hospital, University of Zurich, Switzerland.

³Computer Vision Lab, ETH Zurich, Switzerland.

⁴Integrated System Laboratory, ETH Zurich, Switzerland.

⁵Institute of Medical Genetics and Pathology, University Hospital Basel, Switzerland.

Jiqing.Wu@unibas.ch, ingrid.berg@biol.ethz.ch,

{yawei.li, ender.konukoglu}@vision.ee.ethz.ch,

*Corresponding Author: Viktor.Koelzer@usb.ch

Abstract

Holistic 3D modeling of molecularly defined brain structures is crucial for understanding complex brain functions. Emerging tissue profiling technologies enable the construction of a comprehensive atlas of the mammalian brain with sub-cellular resolution and spatially resolved gene expression data. However, such tera-scale volumetric datasets present significant computational challenges in understanding complex brain functions within their native 3D spatial context. Here, we propose the novel generative approach **Tera-MIND**, which can simulate **Tera**-scale **M**ouse **bra**INs in 3D using a patch-based and boundary-aware **D**iffusion model. Taking spatial transcriptomic data as the conditional input, we generate virtual mouse brains with comprehensive cellular morphological detail at teravoxel scale. Through the lens of 3D *gene-gene* self-attention, we identify spatial molecular interactions for key transcriptomic pathways in the murine brain, exemplified by glutamatergic and dopaminergic neuronal systems. Importantly, these *in-silico* biological findings are consistent and reproducible across three tera-scale virtual mouse brains. Therefore, Tera-MIND showcases a promising path toward efficient and generative simulations of whole organ systems for biomedical research. Project website: <https://musikisomorphie.github.io/Tera-MIND.html>

1 Introduction

Recently, a network of researchers [47, 49, 21, 35] has reached a groundbreaking milestone by charting the first complete cellular atlas of the adult mouse brain, the most extensively studied animal model in neuroscience. Using advanced spatial transcriptomics methods [3, 25, 5] capable of profiling molecularly defined brain anatomy and morphology at sub-cellular resolution, the collective studies established foundational resources and datasets, providing an unprecedented framework for systematically exploring the molecular-driven spatial organization of the mammalian brain. Consequently, this landmark achievement opens the door for next-generation investigations into intricate brain functions characterized by exceptional spatial complexity. However, these tera-scale volumetric datasets, including spatial molecular data (e.g., mRNA readouts acting as proxies for gene expression) and paired morphological bioimages, pose substantial computational challenges [45] for *in-silico* modeling of the mouse brain. Integrating spatial gene expression with 3D brain morphology to uncover functional relationships at whole organ scale remains an open challenge.

Meanwhile, generative artificial intelligence (GenAI) has emerged as a transformative tool for automating visual content creation and manipulation [4, 48]. Given a text prompt that describes the desired visual content, GenAI models [14, 15] are able to produce highly realistic images and videos [32, 30] with remarkable efficiency. In biomedical research, the applications of GenAI have gained domain-specific recognition in various areas such as digital histopathology [2], drug screening [43, 20], and molecule design [4]. However, the direct application of existing GenAI methods to whole organ simulation has currently remained infeasible due to technological limitations. Developed upon the framework of Generative Adversarial Nets (GAN) [14], the GigaGAN [19] model was trained on 96-128 A100 GPUs to synthesize $4,096 \times 4,096$ color images. Using up to 6,144 H100 GPUs, Movie Gen [31], a diffusion-based model [15], achieved video generation results with $1,092 \times 1,080 \times 256$ spatial-temporal resolution. In comparison, even after image registration and quality control, the mouse brain atlas remains at tera-scale volume, consisting of 100 whole slide images (WSIs; $0.108\mu\text{m}/\text{pixel}$) paired with size-matched gene expression arrays, each with a spatial resolution of $73,216 \times 105,984$. This immense data scale of WSIs (e.g., $73,216 \times 105,984 \times 100 = 0.77 \times 10^{12}$ voxels) as well as gene expression arrays significantly amplifies the computational demands associated with GenAI modeling of a virtual mouse brain.

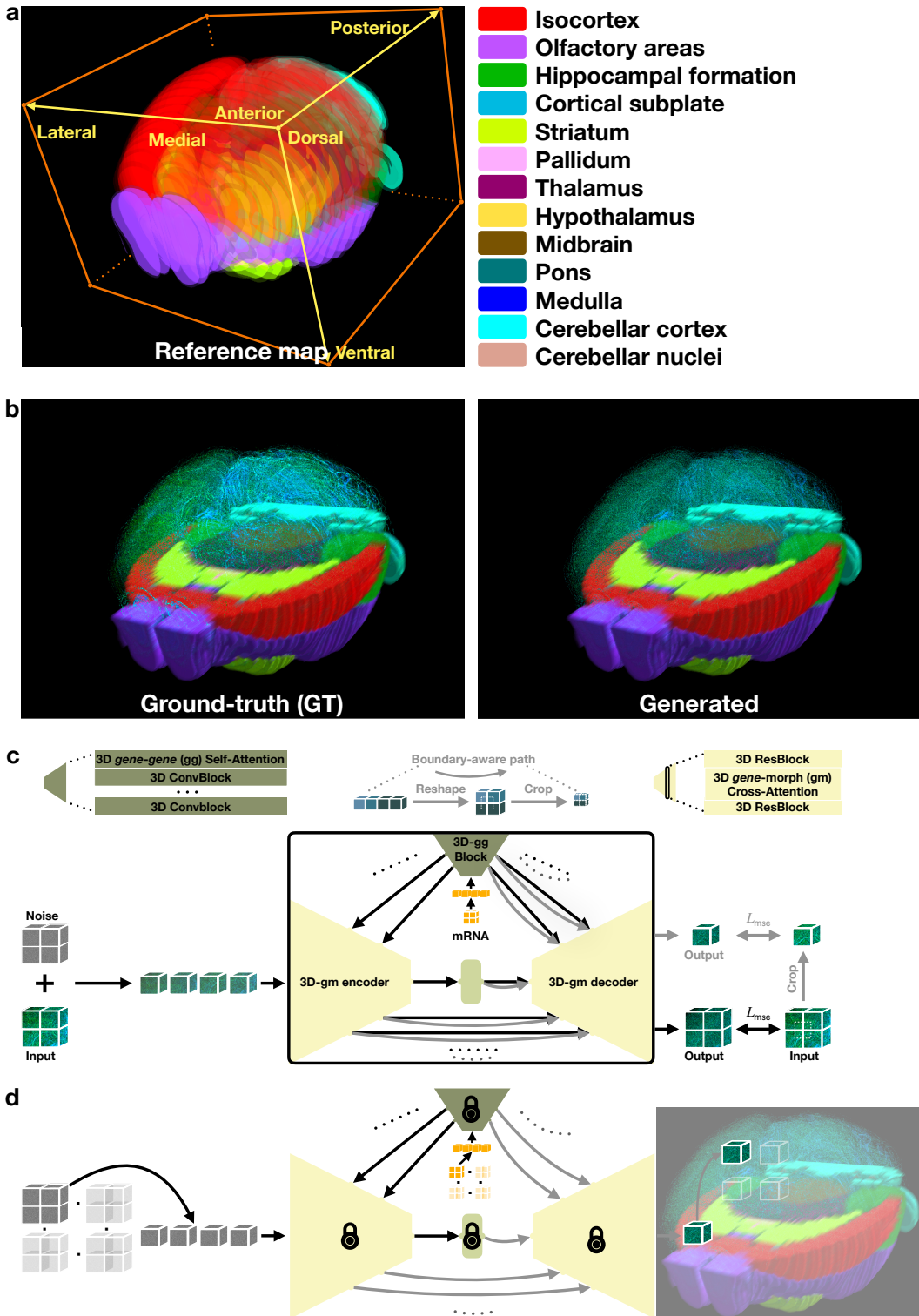
Addressing memory bottlenecks in high-resolution image generation has previously motivated the development of patch-based approaches [22, 23, 46, 28, 12], which enforce boundary consistency [45] between generated neighboring patches. Similar to many standard GenAI models, these approaches can also leverage the interplay between textual and visual modalities and create desired visual content conditioned on text prompts. While this design choice has shown remarkable success in natural image synthesis and artistic content creation, it is suboptimal for biomedical applications – particularly for the accurate 3D molecular-driven reconstruction of mammalian brains. The inherent complexity of brain morphology controlled by spatial molecular interactions demands a generative framework that can capture molecular-to-morphology spatial associations with precision. In response to these challenges, we propose **Tera-MIND**, a novel GenAI approach designed for the paired data structure of spatial mRNA arrays (gene expression, prompts) and WSIs (brain morphology, bioimages). Specifically, Tera-MIND employs a newly introduced patch-based and boundary-aware diffusion model, which allows the reconstruction of tera-scale mouse brains with high fidelity. Owing to the patch-wise training and inference paradigm, Tera-MIND models *in-silico* mammalian brain(s) with computational efficiency. As a result, the whole simulation process can be efficiently executed on a single DGX A100 machine, significantly lowering hardware demands while maintaining scalability for tera-scale data processing. This efficiency underscores the potential wide applicability of Tera-MIND for biomedical applications. Our contributions can be summarized as follows:

- By conditioning on 3D spatial gene expression as the input prompt, Tera-MIND enables the seamless generation of *in-silico* mouse brains at the scale of 0.77 teravoxels. Moreover, our approach accurately preserves fine-grained morphological structures across cellular, tissue, and slice-wise scales, supporting detailed exploration and comparison of brain architecture.
- Leveraging 3D *gene-gene* self-attention mechanisms, we quantify and visualize spatial molecular interactions of key pathways that contribute to fundamental brain functions, including those involved in glutamatergic (*Slc17a6* and *Slc17a7*) and dopaminergic (*Nr4a2* and *Th*) neuronal systems.
- Lastly, the *in-silico* biological findings obtained by Tera-MIND can be efficiently reproduced across three tera-scale virtual mouse brains. This confirms the robustness and reliability of Tera-MIND for biomedical applications.

2 Results

2.1 Model overview of Tera-MIND

To resolve the high-volume computational demand, we develop a novel patch-based and boundary-aware diffusion model **Tera-MIND**, designed for the scalable and seamless generation of teravoxel mouse brains (See Fig. 1 (a, b)). Considering the spatial linkage of gene expression variability and brain morphology, we propose to modulate a 3D *gene-morph* (gm) UNet using a tailored 3D *gene-gene* (gg) block. By feeding the spatial gene expression array (input prompt) to the 3D-gg block, we achieve the sub-cellular control of brain morphology generation through the 3D-gm



UNet, please see Fig. 1 (c) for more illustrations. To assess the role of individual genes and their relationships within gene groups, the proposed 3D *gene-gene* block includes a 3D self-attention layer that learns the *gene-gene* interaction level within the native 3D spatial context. Following the attention architecture introduced in Diffusion Transformer (DiT) [30], we then inject learned *gene-gene* attention representations into the 3D *gene-morph* cross-attention block, eventually modulating brain morphology generation using 3D-gm UNet. In addition to the patch-wise reconstruction path (black arrows in Fig. 1 (c, d)), we further introduce a boundary-aware path (gray arrows in Fig. 1 (c, d), please see also [12]) to output center-cropped brain morphology patches. Specifically, the training process involves randomly cropping paired n -plex gene expression arrays and their corresponding morphological bioimages from training mouse brain atlas(es) [47]. Our patch-based approach thus enables efficient training of the Tera-MIND model on $2 \times 40\text{GB}$ A100 GPUs. During inference, Tera-MIND supports the seamless generation of unseen mouse brain(s) with high fidelity, while the hardware requirement remains moderate, *e.g.*, 7 days on a single DGX machine with $8 \times 40\text{GB}$ A100 GPUs. For model details we refer interested readers to the [Methods](#) section and [code repository](#).

2.2 Tera-MIND enables accurate generation of tera-scale mouse brain(s) by spatial gene expression.

Consistent with the primary analysis described in [49, 47], which was conducted on a comprehensive brain atlas of a P56 female adult mouse, we present **main** simulation results of Tera-MIND based on the same brain atlas. The holistic 3D comparison between the ground truth (GT) and our generation result is illustrated in Fig. 1 (b) and Fig. 2 (a). Given 3D spatial gene expression data as an input, Tera-MIND achieves the faithful and comprehensive reconstruction of 3D brain morphology, as captured by a sequential stack of **DAPI** and **PolyT**-stained WSIs. Specifically, the generated mouse brain has the same teravoxel scale as GT, *e.g.*, $73,216 \times 105,984 \times 100 = 0.77$ teravoxels. At the level of individual WSIs (Fig. 2 (b, c)), Tera-MIND exhibits high-quality generation across multiple scales, including cellular, regional, and slice-wise morphological organization. Within distinct brain regions, such as the olfactory areas, isocortex, and cerebellar cortex, Tera-MIND accurately reconstructs complex morphological structures while preserving native cellular distributions. These results highlight the robustness of Tera-MIND for reconstructing 3D brain morphology directly from spatial gene expression profiles.

Complementary to the side-by-side qualitative comparisons, we perform thorough quantitative analyses of the reconstruction quality by Tera-MIND. For a fair and systematic assessment of the biomedical-specific outputs, we report not only commonly used metrics such as Peak Signal-to-Noise Ratio (PSNR) and Structural Similarity Index Measure (SSIM), but also include patch-based morphometric analyses of nuclear size and cell number. These domain-specific metrics are critical for evaluating the biological fidelity of reconstructed brain morphology at the cellular level. Then, we perform quantitative evaluation on Tera-MIND in comparison to state-of-the-art (SOTA) methods CoCoGAN [22], InfinityGAN [23], IST-editing [42], SinFusion [28], Patch-DM [12], *etc.* Overall, Tera-MIND achieved superior performance in terms of better PSNR and SSIM scores. Furthermore, experimental results reported in Fig. 2 (e) demonstrated marginal morphometric discrepancies between GT cellular patches and those generated by Tera-MIND, which are consistent with the results of stratified patch examples shown in Fig. 2 (e). Using spatial gene expression as the input prompt, these analyses confirm that Tera-MIND reliably reconstructs brain morphology across multiple scales, from cellular and regional structures to whole-brain organization. This consistent performance across scales highlights the efficacy of our approach for accurately capturing the complex spatial patterns of 3D brain morphology.

2.3 Tera-MIND identifies biologically relevant *gene-gene* interactions within native 3D spatial organizations.

To explore the role of individual genes and their interactions in governing the reconstruction of the 3D mouse brain, we analyze the learned 3D *gene-gene* attention map and focus on two critical neuronal systems: glutamatergic (GLUT) and dopaminergic (DOPA) signaling pathways. These examples demonstrate that Tera-MIND is capable of capturing biologically relevant spatial molecular interactions that are essential for the structural and functional interplay of mammalian brains.

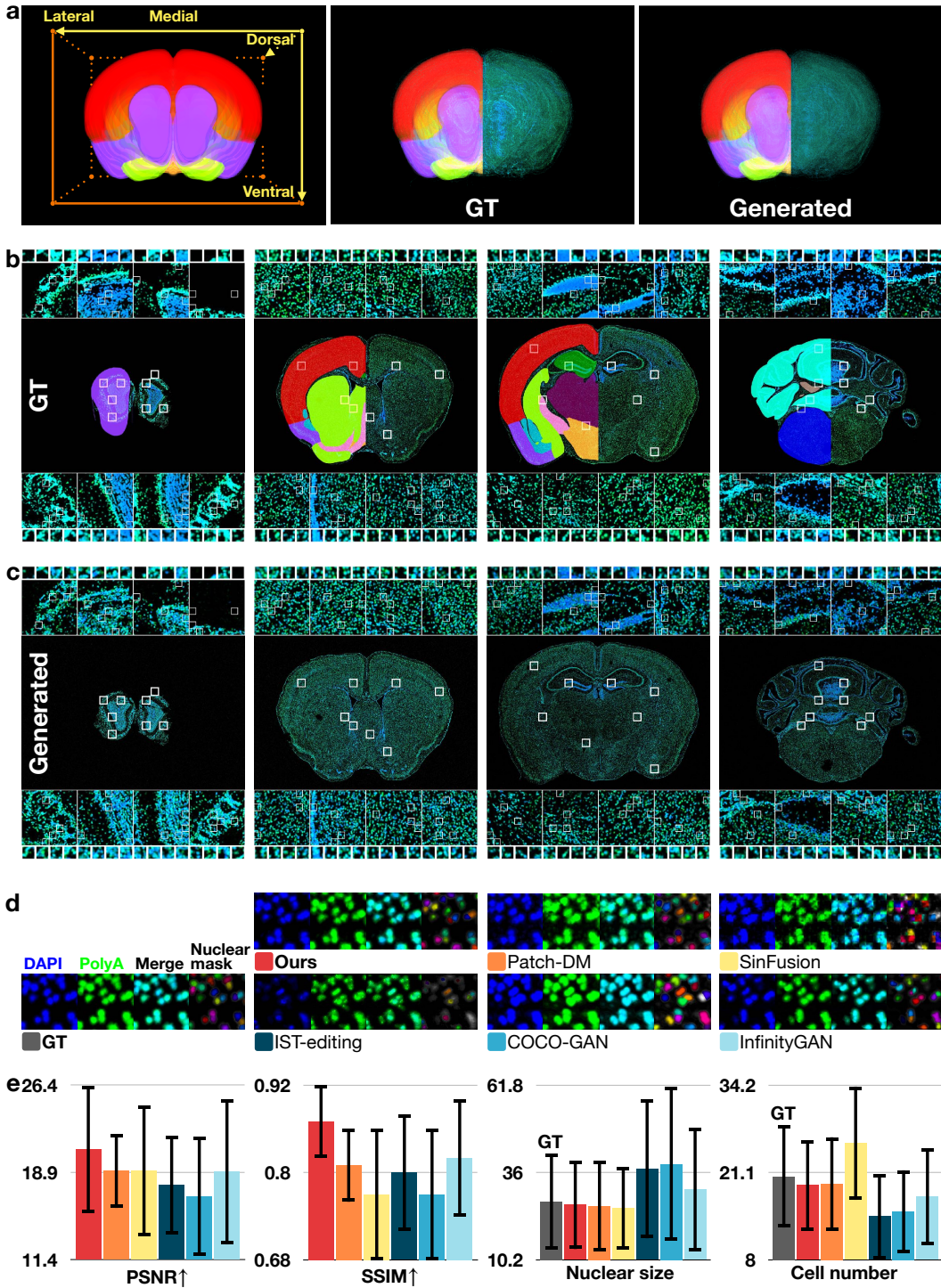


Figure 2: The visual and quantitative comparison of mouse brain generation (Main result). **a.** The 3D map of major brain regions (left), GT (middle), and the generated mouse brain (right) of the atlas used in the primary analysis [47]. **b.** The cell- and region-level visualization of GT mouse brain WSIs in selected brain slices. For (a) and (b), the 3D/2D reference maps of brain regions are overlaid to aid in the navigation of brain structures. **c.** The cell- and region-level visualization of generated mouse brain WSIs. **d.** The visual comparison of exemplar cellular regions (1024×1024) between Tera-MIND and state-of-the-art (SOTA) patch-based models. From left to right, the image stack displays individual DAPI, PolyA, merged channels, and nuclear masks obtained using Cellpose [29]. **e.** Quantitative comparison of image generation quality between Tera-MIND and SOTA methods. This includes mean and standard deviation scores for widely-used image quality metrics, such as PSNR and SSIM, alongside domain-specific scores like patch-based nuclear size and cell count. For a more in-depth analysis, we encourage readers to zoom in on the visual results for clearer comparisons.

2.3.1 GLUT neuronal system

Glutamate is the primary excitatory neurotransmitter in the brain and plays a pivotal role in a wide range of brain functions [38]. The vesicular glutamate transporters VGLUT1 and VGLUT2, encoded by *Slc17a7* and *Slc17a6* resp., regulate extracellular glutamate concentrations and synaptic signaling [38, 40]. Moreover, the expression level of VGLUTs impacts the amount of glutamate loaded into vesicles and released, thereby affecting neurotransmission [41]. Changes in VGLUT expression levels have been associated with various neurological pathologies such as schizophrenia, neuropathic pain, and ischemia [24, 34]. In adult mouse brains, spatial expression patterns of VGLUT1 and VGLUT2 are generally complementary but not exclusive [41]. Specifically, *Slc17a7* (VGLUT1) is broadly expressed in the cerebral cortex, cerebellar cortex, hippocampus, and thalamus, etc., while *Slc17a6* (VGLUT2) can be found in subcortical regions such as the thalamus and spinal cord. As shown in Fig. 3 (a, b), spatial expression patterns of these transporters are accurately mapped in 3D space and align with prior studies [47, 49], which justifies the registration process of brain atlas utilized in this study. Interestingly, the 3D *gene-gene* attention map learned by Tera-MIND reveals heterogeneous and widespread attention signals for the spatial interaction between *Slc17a6* and *Slc17a7* (See also Fig. 3 (a) and (d)). Since both transporters collectively contribute to the regulation of synaptic vesicle glutamate content in those overlapped regions, the spatial *Slc17a6-Slc17a7* attention signal (Fig. 3 (a, d)) and their positive correlation to the gene expression level (Fig. 3 (c)) likely encapsulate their co-expression patterns and accumulative impact on neurotransmission and regional brain morphology.

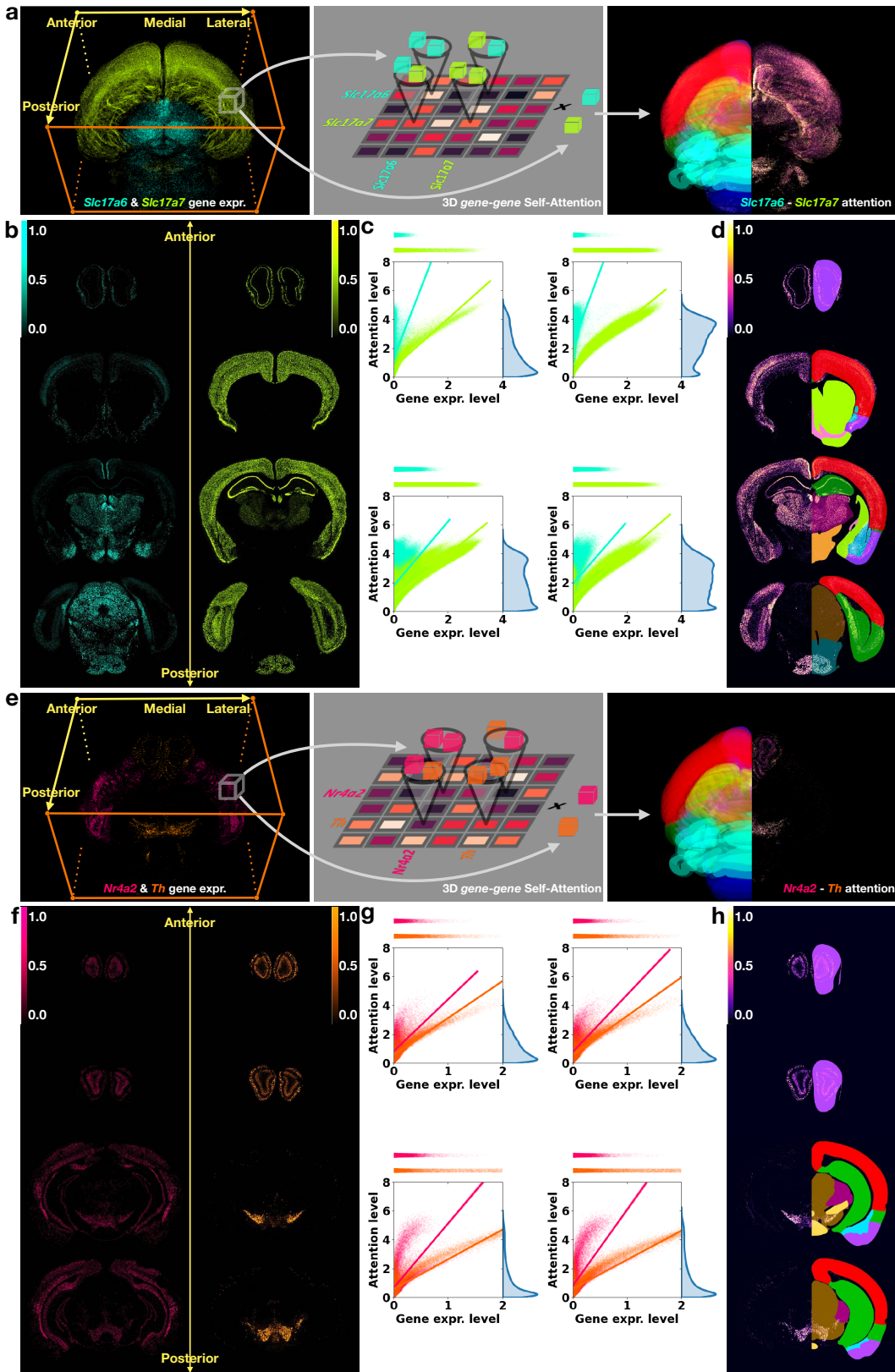
2.3.2 DOPA neuronal system

In dopamine-mediated neuronal signaling, *Nr4a2* (Nurr1) is an important transcription factor that is expressed in several regions of the central nervous system including the substantia nigra (SN), ventral tegmental area (VTA), and olfactory bulb [16]. *Nr4a2* plays a pivotal role in dopaminergic neurons by regulating several key genes (e.g., *Th*) involved in dopamine synthesis, storage, and release. *Th* encodes tyrosine hydroxylase, the rate-limiting enzyme in dopamine synthesis [16]. *Nr4a2* and *Th* expression have been shown to co-localize in areas such as SN, VTA, and olfactory bulb of the mouse brain [33, 13]. Such co-localization patterns have been correctly captured in spatial visualizations presented in Fig. 3 (e, f). Reduced *Nr4a2* and *Th* expression have been associated with Parkinson's disease [18, 11], a common neurodegenerative disorder with loss of dopaminergic neurons in the SN, leading to dopamine deficiency and motor function impairments [18, 11]. This has also been observed in mice after deletion of *Nr4a2* in mature dopaminergic neurons [10]. In the analysis of DOPA neuronal signaling, Tera-MIND uncovers distinct and strong *Nr4a2-Th* attention signals in the SN, VTA, and olfactory bulb, where both genes play a central role in regulating dopaminergic functions. As shown in Fig. 3 (e, g, h), the 3D *gene-gene* attention map reveals a spatially aligned interaction between *Nr4a2* and *Th* that reinforces their roles in the molecular regulation of dopaminergic pathways and cellular anatomical structures.

2.4 Tera-MIND achieves reproducible and robust simulation results on three tera-scale virtual mouse brains.

In addition to the main mouse brain discussed above, two additional P56 adult mouse brains – one male and one female – were profiled in previous studies [47, 49] for supporting analyses, as illustrated in Fig. 4 (a) (middle and right). To rigorously evaluate the reproducibility and robustness of our findings, we extend the same simulation experiments conducted on the **main** mouse brain to both supporting mouse brains (**supp (m)** and **supp (f)**).

Morphology generation: As illustrated in Fig. 4 (a, b), the side-by-side visual comparisons between our generated and GT results demonstrate convincing reconstructions of brain morphology on all three tera-scale mouse brains. Consistent with the main generation results (Fig. 1 (b) and the left plots of Fig. 4 (a, b)), our supporting experiments highlight competitive and reliable 3D and slice-wise image generation quality, as elaborated by the holistic and multi-scale visualization shown in the middle and right plots of Fig. 4 (a, b). For quantitative evaluation, Tera-MIND is benchmarked against seven SOTA methods COCO-GAN [22], InfinityGAN [23], MS-PIE [46], SST-editing [44], IST-editing [42], SinFusion [28], and Patch-DM [12]. Complementary to PSNR and SSIM scores, we incorporate the spatial Fréchet Inception Distance (sFID) [26], which prioritizes spatially relevant evaluations by rewarding image distributions that preserve coherent spatial structures. Across all



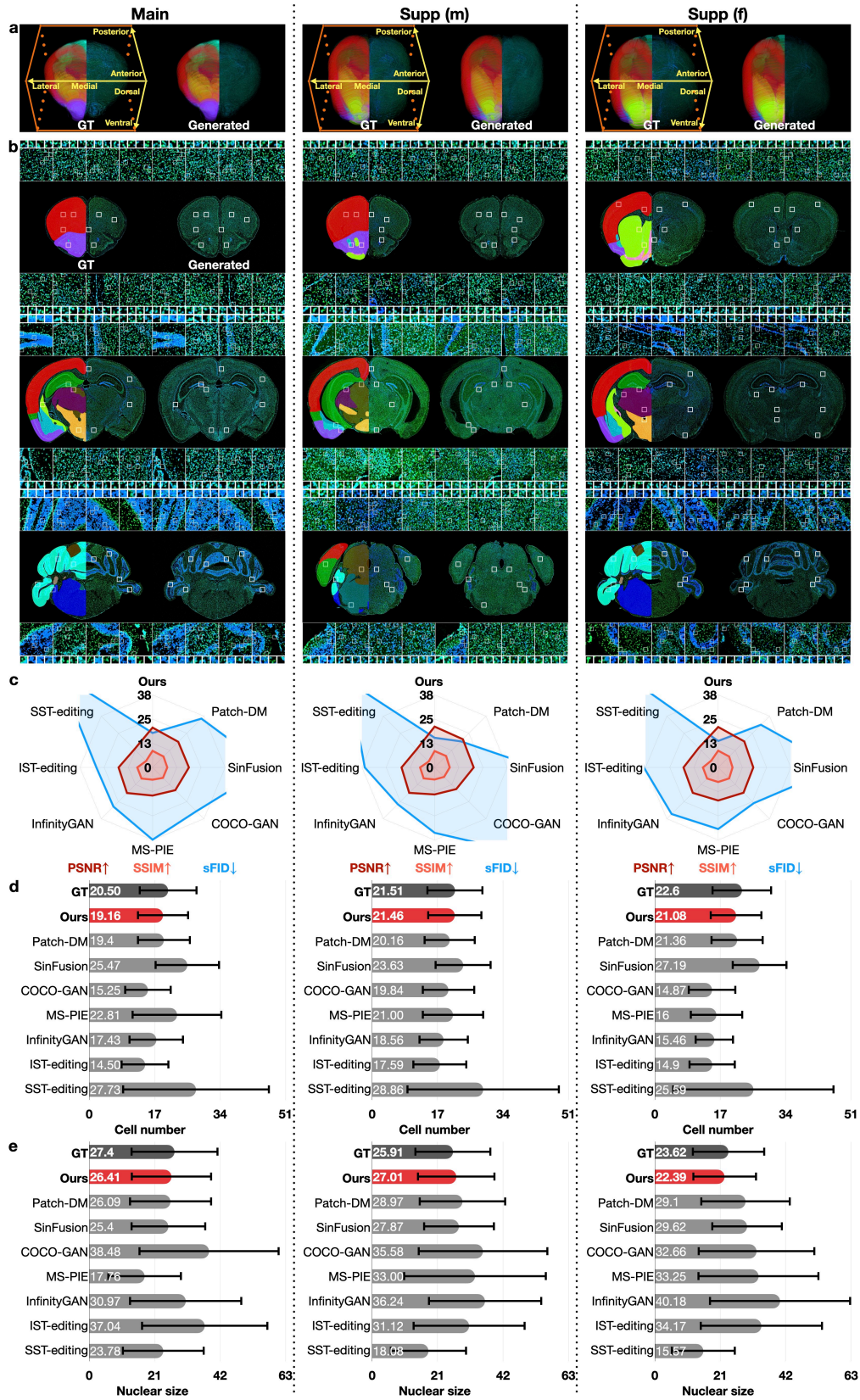


Figure 4: The visual and quantitative comparison for the main and supp mouse brain results. **a.** The holistic 3D comparison between the generated and GT mouse brain, with the brain region map provided on the left for structural guidance. Note that all three generated mouse brains have the same 0.77×10^{12} voxel scale. **b.** The cell- and region-level visualizations of WSIs for the side-by-side comparison between the generated and GT mouse brain. **c.** The quantitative comparison of generation quality between Tera-MIND and SOTA methods, as measured by PSNR, SSIM, and sFID. **d.** Compared to the GT results, the quantitative evaluation of cell numbers derived from Tera-MIND and SOTA methods. **e.** Compared to the GT results, the quantitative evaluation of nuclear size derived from Tera-MIND and SOTA methods.

three brain instances, Tera-MIND consistently outperforms competing methods (Fig. 4), in terms of achieving better PSNR, SSIM, and sfID scores. When evaluated on domain-specific metrics such as cell number and nuclear size, Tera-MIND yields minimal distributional discrepancies relative to GT. This highlights its capacity to maintain high-fidelity not only in structural reconstruction but in the reproduction of biologically relevant features.

Pathway identification: In the context of the GLUT pathway, Fig. 5 (a, b) present a highly consistent and spatially comparable localization of *Slc17a6* and *Slc17a7* expression patterns across two independent supporting instances. These expression maps are accurately registered in 3D space and align well with the ones from our main results and previous studies [47, 49]. Similarly as observed in the main results, Fig. 5 (c) and (d) illustrate that Tera-MIND is capable of learning strong and heterogeneous *Slc17a6-Slc17a7* attention levels driven by the positively correlated gene expression levels. This suggests their synergistic and collective roles in regulating neurotransmission and cellular morphology across overlapped regions. Regarding the DOPA pathway, despite the absence of the olfactory bulb in the raw data of the supporting mouse brains, the gene expression patterns of *Nr4a2* and *Th* exhibit a comparable emergence in the SN and VTA regions (See also Fig. 5 (e, f)). Consistent with the main results, we observe reproducible and clear identification of *Nr4a2-Th* attention levels derived from Tera-MIND in the same regions for both supporting mouse brains (Fig. 5 (e, h)). These results confirm a consistent expression pattern of critical genes associated with dopaminergic function in these specific regions. For more comprehensive 3D illustrations of both pathways, we refer interested readers to the side-by-side [video visualizations](#) across all three mouse brain instances.

3 Discussion

In this study, we introduced a novel patch-based diffusion model Tera-MIND for tera-scale mouse brain simulation with high fidelity. Using spatial gene expression as the input prompt, Tera-MIND achieves seamless generation of tera-scale mouse brain(s) under moderate hardware requirements, making it accessible for broader applications in both computational and biomedical research. In comparison to seven cutting-edge methods [22, 23, 42, 28, 12, 44, 46], which are developed upon either the GAN or diffusion framework, we thoroughly presented the overall improved performance achieved by Tera-MIND. Beyond its generation efficiency, Tera-MIND enables the comprehensive analysis of spatial *gene-gene* attention patterns, as exemplified for both GLUT and DOPA neuronal systems. These experimental analyses offer biologically relevant insights into the spatial organization and interaction of gene expression. Specifically, our findings are reported not only on the main mouse instance (**Main**), as primarily presented in [47], but also on two supporting mouse brains (**Supp** (m, f)) to ensure reproducibility and consistency. These results showcase the robustness of Tera-MIND in generating biologically accurate and spatially coherent brain morphologies guided by spatial molecular data.

We acknowledge the limitations of Tera-MIND. The modeling paradigm is fundamentally driven by the molecular-to-morphology spatial associations, which, while powerful, represent a simplified hypothesis of the complex neurological processes. Future refinements of this methodology could address this challenge by incorporating additional spatiotemporal data modalities, such as epigenomic, transcriptomic, proteomic, and (immuno-)histological information from diverse developmental and pathological contexts, along with adaptations for human tissue analysis. With these enhancements, Tera-MIND can further advance research into the spatial dynamics of gene expression and the cellular alterations associated with complex human (neurological) diseases [39].

In conclusion, the development of virtual replicas of entire biological organisms using GenAI, referred to as generative digital twins (GDTs [45]) and exemplified by Tera-MIND in this study, opens new avenues for high-throughput biomedical simulation with minimal ethical concerns. This methodology offers a cost-effective and scalable alternative for preclinical testing of therapeutic strategies. Lastly, the potentially wide applicability of GDTs on human samples aligns with the principles of animal welfare by supporting the replacement, reduction, and refinement (3R) of animal use in laboratory research, providing a promising algorithmic tool for ethically responsible biomedical innovation.

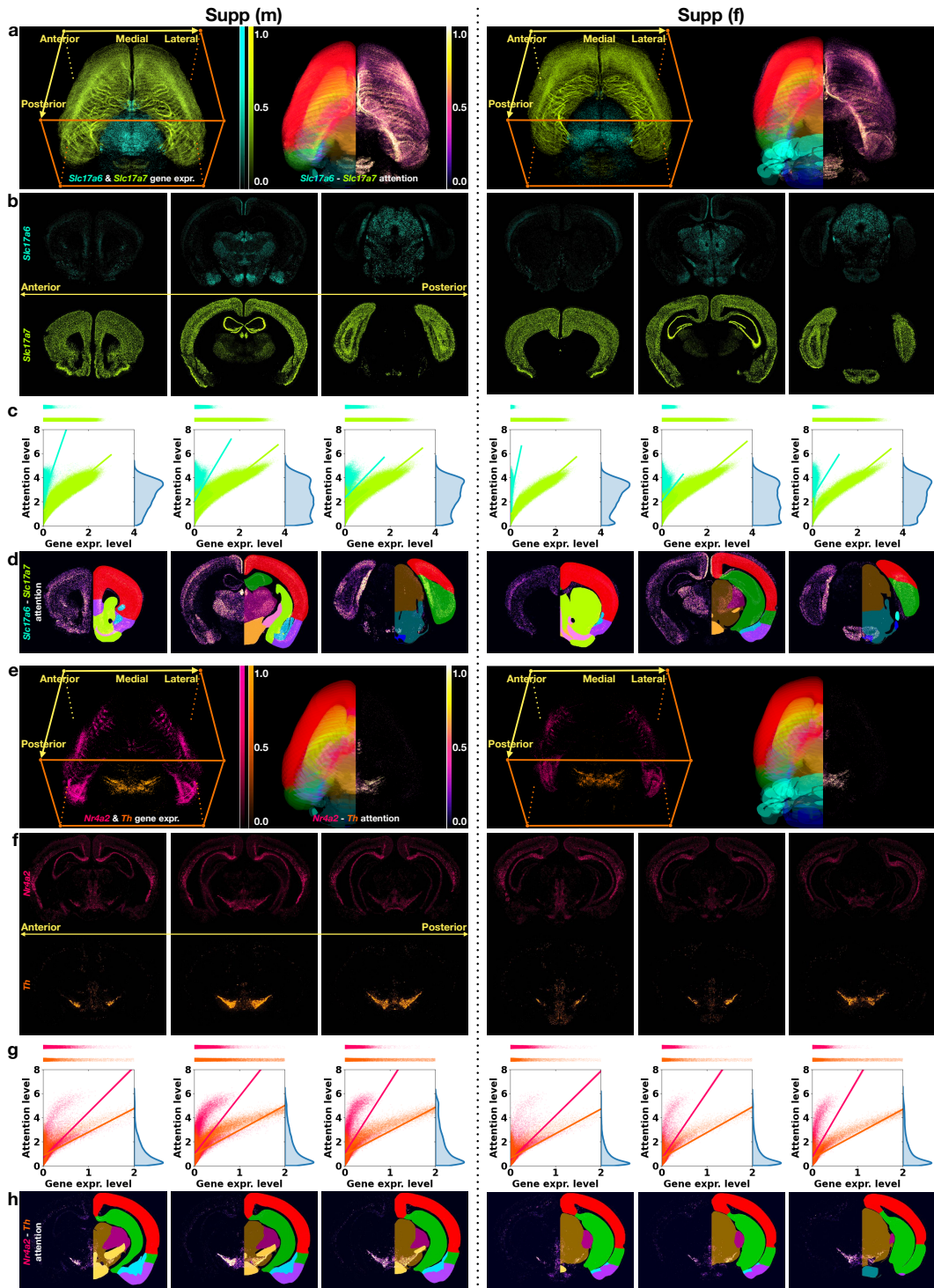


Figure 5: The visualization of gene-gene interaction for GLUT and DOPA neuronal systems (Supp (m) and (f) results). **a.** The 3D visualization of *Slc17a6* and *Slc17a7* gene expression (left) and the 3D visualization of *Slc17a6-Slc17a7* attention (right). **b.** The WSI visualization of *Slc17a6* and *Slc17a7* gene expression (expr.). **c.** The trending line showing the relationship between gene expr. and attention level for both *Slc17a6* and *Slc17a7*. **d.** The WSI visualization of *Slc17a6-Slc17a7* attention level. **e.** The 3D visualization of *Nr4a2* and *Th* gene expression (left) and the 3D visualization of *Nr4a2-Th* attention (right). **f.** The WSI visualization of *Nr4a2* and *Th* gene expression (expr.). **g.** The trending line showing the relationship between gene expr. and attention level for both *Nr4a2* and *Th*. **h.** The WSI visualization of *Nr4a2-Th* attention level. For a clearer visualization, gene expr. and attention levels are normalized to the range [0, 1] for both GLUT and DOPA pathways.

4 Methods

4.1 Spatial mRNA data as 3D ‘images’

Biological processes are inherently spatial [3]. The spatial molecular organization of the mammalian brain plays a decisive role in defining brain functionality and its dysfunction in disease. Recognizing the importance of spatial context, we leverage spatial mRNA readouts [47, 49] as 3D ‘images’, which are paired with corresponding 3D morphological bioimages. Unlike conventional data representations, such as 1D gene expression vector [8, 37], text description [6], graph-based structure [17, 1], or genomic sequence [27], our simple and vision-driven data format naturally maintains the 3D localization of molecular features, facilitating the holistic modeling of intrinsic spatial organizations that underpins brain function and dysfunction.

4.2 Spatial paired data processing

In prior studies [47, 49], three comprehensive and high-resolution brain atlases have been made publicly available ¹. For each brain slice, there exists a large multiplex gene expression table and the associated morphological bioimages, as captured by DAPI- and PolyT-stained high-resolution WSIs ($0.108\mu\text{m}/\text{pixel}$). Given the coordinate misalignment across available brain slices, we start the data processing by image registration. To maintain the original scale of raw data and for the sake of molecular data conversion, the registration-derived transformation matrix is required for our customized data processing. To this end, we employ the ABBA software [7] to perform the brain atlas registration, which allows us to access individual transformation matrices S . By applying the inverse S^{-1} on the raw molecular and morphological data resp., we obtain the updated (large) gene expression table with transformed coordinates and the transformed WSI. For all brain slices, its transformed gene expression table is then converted to a sparse array, which has the same $73,216 \times 105,984$ spatial resolution as the corresponding transformed WSI. Specifically, we employ the same processing pipeline on all the available atlases and obtain three sets of gene expression 3D images and associated WSIs. After excluding the brain slices with corrupted image quality and post-processing, we keep 50 slices of paired data for each brain atlas. Note that the processed results have been carefully examined by domain experts to ensure the registration quality. We refer interested readers to App. Fig. 8, 9, 10 (a) for more details. After consecutively stacking 50 slices of gene expression arrays and WSIs resp., we obtain the whole tera-scale paired 3D ‘images’, from which we can collect a large amount of small data pairs (e.g., 128×128) for running the model.

4.3 The proposed Tera-MIND

To faithfully capture the molecular-to-morphology spatial associations, we introduce a 3D *gene-gene* block that learns the spatial gene expression embeddings, which are subsequently integrated into the 3D *gene-morph* (gm) UNet to control the morphological reconstruction process (Fig. 1 (c, d)). Inspired by DIT [30, 50], we apply newly designed spatial attention blocks to our model architecture.

3D *gene-gene* (gg) self-attention. Instead of 1D conditional embeddings learned from textual descriptions, we use the 3D-gg self-attention layer to process the 3D gene expression array used as the conditional prompt. Let $\mathbf{g} \in \mathbb{R}^{n \times d}$ be a n -plex 3D gene expression array with the spatial dimension $d = \text{width} \times \text{height} \times z$, where z denotes the number of stacked slices from which the gene expression is extracted. Then, we have

$$\begin{aligned} \mathbf{Q}_g &= \text{RMSNorm}(\mathbf{gW}_q), \quad \mathbf{K}_g = \text{RMSNorm}(\mathbf{gW}_k), \\ \mathbf{Attn}_g &= \underbrace{\text{nn.Softmax}\left(\frac{\mathbf{Q}_g \mathbf{K}_g^T}{d}\right)}_{\mathbf{Attn}_{gg}} \mathbf{gW}_v, \quad \text{where } \mathbf{V}_g = \mathbf{gW}_v. \end{aligned} \quad (1)$$

Here, $\mathbf{W}_{\{q,k,v\}} \in \mathbb{R}^{d \times d}$ are learnable weights and \mathbf{Attn}_{gg} is the derived spatial *gene-gene* attention reported in Fig. 3 and 5. After stepwise 3D convolutional upscaling on the \mathbf{Attn}_g , we have the sequential of 3D gene features $\mathbf{g}_i \in \mathbb{R}^{d_i \times n_i}$ for $i = 1, \dots, l$, with the increasing spatial resolutions by the magnitude of 2.

¹<https://download.brainimagedatabase.org/aa/79/aa79b8ba5b3add56/>

3D gene-morph (gm) cross-attention. To integrate the learned g_i into the reconstruction of morphological images by 3D-gm UNet, we inject selected g_i to the corresponding layer of encoder and decoder, which process morphological presentations $\mathbf{m}_i \in \mathbb{R}^{d_i \times c_i}$ at the same spatial resolution d_i . First, we obtain the spatial adaptive coefficients $\text{Scale}_{g_i}, \text{Shift}_{g_i}, \text{Gate}_{g_i} \in \mathbb{R}^{d_i}$ and gene embedding $\text{Embed}_{g_i} \in \mathbb{R}^{d_i}$ by inputting the g_i to the AdaLN [30, 50] block containing nn.SiLU and nn.Linear layers. Then, we have

$$\begin{aligned} \text{Ada}_{\mathbf{m}_i} &= \text{RMSNorm}(\mathbf{m}_i) \cdot (\text{Scale}_{g_i} + 1) + \text{Shift}_{g_i}, \\ \mathbf{P}_{\mathbf{m}_i} &= \mathbf{m}_i + \text{Gate}_{g_i} \text{nn.Softmax}\left(\frac{\mathbf{Q}_{\text{Ada}_{\mathbf{m}_i}} \mathbf{K}_{\text{Ada}_{\mathbf{m}_i}}^T}{c_i}\right) \mathbf{V}_{\text{Embed}_{g_i}}, \end{aligned} \quad (2)$$

where $\mathbf{Q}_{\text{Ada}_{\mathbf{m}_i}}$ and $\mathbf{K}_{\text{Ada}_{\mathbf{m}_i}}$ are query and key representations of $\text{Ada}_{\mathbf{m}_i}$, $\mathbf{V}_{\text{Embed}_{g_i}}$ is the value vector of Embed_{g_i} . For both attention blocks, we use the Pytorch implementation of flash attention-2 [9] to improve computational efficiency and reduce memory cost.

Boundary-aware path. Following the denoising diffusion framework [15], we implement the forward process by gradually adding Gaussian noise to the 3D image patches \mathbf{m} extracted from WSIs at timestep t , which gives us noisy image patches \mathbf{m}_t . Using 3D-gm UNet, we then parameterize the denoising function $\epsilon_\theta(\mathbf{m}_t, t)$ to reverse the process. Similar as [12] and along with the standard denoising process, we supply an additional boundary-aware denoising path to impose the boundary consistency on the center-cropped patches. Therefore, our training objective is determined to be $\|\epsilon_\theta(\mathbf{m}_t^1, t) - \epsilon_1\|^2 + \|\epsilon_\theta(\mathbf{m}_t^2, t) - \epsilon_2\|^2$, where \mathbf{m}_t^1 is the stack of small patches extracted from the input data and \mathbf{m}_t^2 is the center-cropped patch (See also Fig. 1 (c)). During the inference, we only use the boundary-aware path to generate image patches without stitching artifacts.

Model training. Among available mouse brain atlases, previous studies [47, 49] reported the primary results on the P56 female mouse brain (**Main**) including all the major brain regions (Fig. 1 (b)), while the additional P56 male and female mouse brains (**Supp (m), (f)**) that preserve most of the brain regions (Fig. 3 (a)) are used for supporting analyses. Following this experimental setup and to avoid overfitting, we report our primary generation result on the main mouse brain while taking the supp (m) and (f) mouse brains as the training data. Moreover, we filter out the genes that are present across three instances and obtain the 279-plex gene expression array for training (App. Fig. 8 (e)). In addition to the main results reported in Fig. 1, 2, we conduct (unseen) generation experiments on the supporting mouse brains for the sake of reproducibility and consistency. Since supp (m) and (f) are processed using the same protocol with the identical 500-plex gene list (App. Fig. 9, 10 (e)), we take one ‘supp’ brain for training and the other unseen ‘supp’ brain for testing, and vice versa. Given the small distribution shift between supporting brain instances, this setup thus complements the challenging main experiment, which presents a large distribution gap between the training (supp (m, f)) and testing (main) data.

Model inference. After completing the model training, we run the tera-scale brain generation in a patch-wise manner. To ensure both computational feasibility and generation fidelity, we employ the Denoising Diffusion Implicit Models (DDIM) [36] approach for accelerated sampling and high-quality image synthesis. Given the significant GPU memory constraints associated with storing an entire mouse brain, the collection of generated patches is instead temporarily offloaded to the hard drive during each sampling step. These intermediate results are then utilized for the subsequent step. The patch-wise generation framework is inherently parallelizable, enabling efficient resource utilization. On a single NVIDIA A100 DGX system, the entire generation process for a tera-scale mouse brain can be completed within seven days. This demonstrates the scalability and practicality of Tera-MIND for handling large-scale 3D biomedical datasets.

4.4 Ablative studies

To assess the impact of key design choices in Tera-MIND, we discuss ablative results based on three critical factors: the number of slices used to extract 3D training data pairs, the spatial resolution of image patches, and the number of sampling steps. In line with the previous evaluations, both general metrics (PSNR and SSIM) and domain-specific metrics (Nuclear size and Cell number) are reported for a more comprehensive analysis.

For all three brain instances, optimal quantitative performance has been achieved when the slice number was set to 2. This is supported by the fact that neighboring slices are separated by a relatively

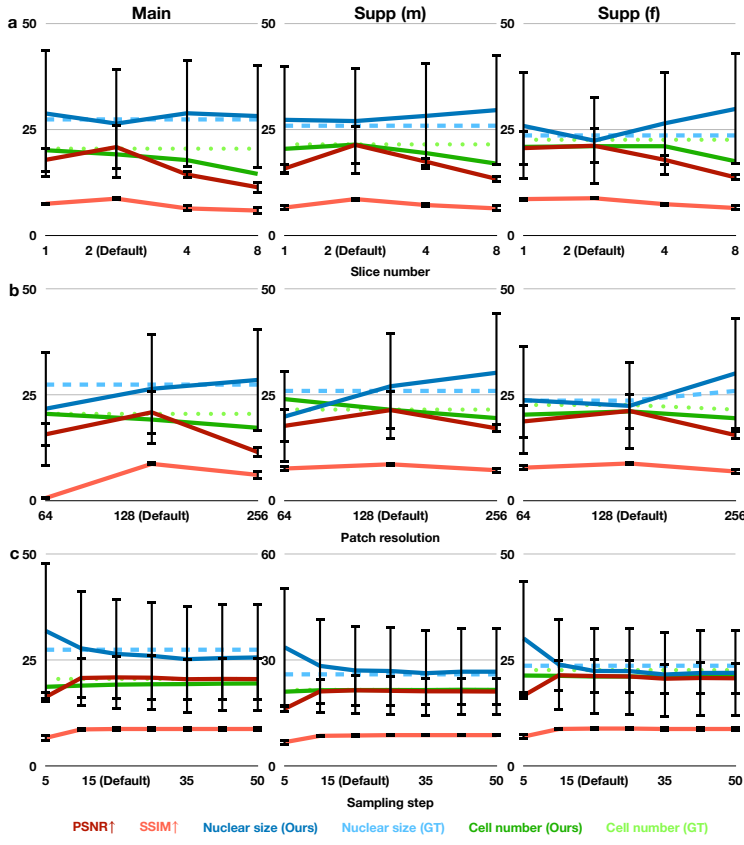


Figure 6: **The ablative results on the main and supp (m, f) mouse brains.** **a.** Quantitative performance metrics evaluated across varying slice counts. **b.** Quantitative performance metrics assessed at different spatial resolutions. **c.** Quantitative performance metrics reported for varying sampling steps.

large interval, ranging from $100\mu\text{m}$ to $200\mu\text{m}$ [47]. When compared to the neighboring pixels, which have a physical size of $0.108\mu\text{m}$ per pixel, the morphological context extracted from more neighboring slices is very likely saturated, as illustrated in Fig. 6 (a). Besides, in comparison to the 2D image training paradigm when the slice number equals 1, our proposed 3D modeling can further learn the cross-slice interaction patterns between neighboring slices. For instance, App. Fig. 7 highlights the consistent spatial *Nr4a2-Th* interaction patterns pinpointed in the very SN and VTA regions across three simulated mouse brains. These results substantiate the superiority of the proposed 3D modeling for the whole biological entity.

Additionally, we explore the effect of varying image patch resolution, ranging from 64×64 to 256×256 (Fig. 6 (b)). Here, we consider the entire patch size of the input data, rather than using an intermediate cropped patch size. Eventually, we determine that the resolution of 128×128 yields the best performance. This choice aligns with the previous Patch-DM study[12], where the whole patch resolution was identified as 128 by default.

Finally, we examined the impact of the DDIM sampling step, weighing the trade-off between computational cost and performance. As shown in Fig. 6 (c), the optimal sampling step for Tera-MIND is determined to be 15. Beyond this point, additional steps lead to saturated improvements in performance, underscoring the cost-effectiveness of this choice.

Data availability

All three mouse brain atlases, including the spatially resolved mRNA table and matched DAPI- and PolyT-stained WSIs for each brain slice, are accessible via <https://download.brainimagelibrary.org/aa/79/aa79b8ba5b3add56/>.

Code availability

The Python implementation used to train the model and reproduce the simulation results can be accessed via <https://github.com/CTPLab/Tera-MIND>.

References

- [1] Josh Abramson, Jonas Adler, Jack Dunger, Richard Evans, Tim Green, Alexander Pritzel, Olaf Ronneberger, Lindsay Willmore, Andrew J Ballard, Joshua Bambrick, et al. Accurate structure prediction of biomolecular interactions with AlphaFold 3. *Nature*, pages 1–3, 2024.
- [2] Shahd A Alajaji, Zaid H Khoury, Mohamed Elgarib, Mamoon Saeed, Ahmed RH Ahmed, Mohammad B Khan, Tiffany Tavares, Maryam Jessri, Adam C Puche, Hamid Hoorfar, et al. Generative Adversarial Networks in Digital Histopathology: Current Applications, Limitations, Ethical Considerations, and Future Directions. *Modern Pathology*, page 100369, 2023.
- [3] Dario Bressan, Giorgia Battistoni, and Gregory J Hannon. The dawn of spatial omics. *Science*, 381(6657):eabq4964, 2023.
- [4] Hanqun Cao, Cheng Tan, Zhangyang Gao, Yilun Xu, Guangyong Chen, Pheng-Ann Heng, and Stan Z Li. A survey on generative diffusion models. *IEEE Transactions on Knowledge and Data Engineering*, 2024.
- [5] Kok Hao Chen, Alistair N Boettiger, Jeffrey R Moffitt, Siyuan Wang, and Xiaowei Zhuang. Spatially resolved, highly multiplexed RNA profiling in single cells. *Science*, 348(6233):aaa6090, 2015.
- [6] Yiqun Chen and James Zou. GenePT: a simple but effective foundation model for genes and cells built from ChatGPT. *bioRxiv*, pages 2023–10, 2024.
- [7] Nicolas Chiaruttini, Carlo Castoldi, Linda Maria Reque, Carmen Camarena-Delgado, Beatrice Dal Bianco, Johannes Gräff, Arne Seitz, and Bianca Ambrogina Silva. ABBA, a novel tool for whole-brain mapping, reveals brain-wide differences in immediate early genes induction following learning. *bioRxiv*, pages 2024–09, 2024.
- [8] Haotian Cui, Chloe Wang, Hassaan Maan, Kuan Pang, Fengning Luo, Nan Duan, and Bo Wang. scGPT: toward building a foundation model for single-cell multi-omics using generative AI. *Nature Methods*, pages 1–11, 2024.
- [9] Tri Dao. FlashAttention-2: Faster Attention with Better Parallelism and Work Partitioning. In *The Twelfth International Conference on Learning Representations*, 2024.
- [10] Mickael Decressac, Nikolaos Volakakis, Anders Björklund, and Thomas Perlmann. NURR1 in Parkinson disease—from pathogenesis to therapeutic potential. *Nature Reviews Neurology*, 9(11):629–636, 2013.
- [11] Isaac Deng, Frances Corrigan, Guangxi Zhai, Xin-Fu Zhou, and Larisa Bobrovskaia. Lipopolysaccharide animal models of Parkinson’s disease: Recent progress and relevance to clinical disease. *Brain, behavior, & immunity-health*, 4:100060, 2020.
- [12] Zheng Ding, Mengqi Zhang, Jiajun Wu, and Zhuowen Tu. Patched denoising diffusion models for high-resolution image synthesis. In *The Twelfth International Conference on Learning Representations*, 2023.
- [13] YuHong Fu, Yuan Yuan, Glenda Halliday, Zoltán Rusznák, Charles Watson, and George Paxinos. A cytoarchitectonic and chemoarchitectonic analysis of the dopamine cell groups in the substantia nigra, ventral tegmental area, and retrorubral field in the mouse. *Brain Structure and Function*, 217:591–612, 2012.
- [14] Ian Goodfellow, Jean Pouget-Abadie, Mehdi Mirza, Bing Xu, David Warde-Farley, Sherjil Ozair, Aaron Courville, and Yoshua Bengio. Generative adversarial nets. *Advances in neural information processing systems*, 27, 2014.
- [15] Jonathan Ho, Ajay Jain, and Pieter Abbeel. Denoising diffusion probabilistic models. *Advances in neural information processing systems*, 33:6840–6851, 2020.
- [16] Md Jakaria, Md Ezazul Haque, Duk-Yeon Cho, Shofiqul Azam, In-Su Kim, and Dong-Kug Choi. Molecular insights into NR4A2 (Nurr1): an emerging target for neuroprotective therapy against neuroinflammation and neuronal cell death. *Molecular neurobiology*, 56:5799–5814, 2019.
- [17] John Jumper, Richard Evans, Alexander Pritzel, Tim Green, Michael Figurnov, Olaf Ronneberger, Kathryn Tunyasuvunakool, Russ Bates, Augustin Žídek, Anna Potapenko, et al. Highly accurate protein structure prediction with AlphaFold. *nature*, 596(7873):583–589, 2021.
- [18] Lorraine V Kalia and Anthony E Lang. Parkinson’s disease. *The Lancet*, 386(9996):896–912, 2015.

[19] Minguk Kang, Jun-Yan Zhu, Richard Zhang, Jaesik Park, Eli Shechtman, Sylvain Paris, and Taesung Park. Scaling up GANs for Text-to-Image Synthesis. In *2023 IEEE/CVF Conference on Computer Vision and Pattern Recognition (CVPR)*, pages 10124–10134. IEEE, 2023.

[20] Alexis Lamiable, Tiphaine Champetier, Francesco Leonardi, Ethan Cohen, Peter Sommer, David Hardy, Nicolas Argy, Achille Massougbedji, Elaine Del Nery, Gilles Cottrell, et al. Revealing invisible cell phenotypes with conditional generative modeling. *Nature Communications*, 14(1):6386, 2023.

[21] Jonah Langlieb, Nina S Sachdev, Karol S Balderrama, Naeem M Nadaf, Mukund Raj, Evan Murray, James T Webber, Charles Vanderburg, Vahid Gazestani, Daniel Tward, et al. The molecular cytoarchitecture of the adult mouse brain. *Nature*, 624(7991):333–342, 2023.

[22] Chieh Hubert Lin, Chia-Che Chang, Yu-Sheng Chen, Da-Cheng Juan, Wei Wei, and Hwann-Tzong Chen. COCO-GAN: Generation by Parts via Conditional Coordinating. In *Proceedings of the IEEE/CVF international conference on computer vision*, pages 4512–4521, 2019.

[23] Chieh Hubert Lin, Hsin-Ying Lee, Yen-Chi Cheng, Sergey Tulyakov, and Ming-Hsuan Yang. InfinityGAN: Towards Infinite-Pixel Image Synthesis. In *International Conference on Learning Representations*, 2021.

[24] Diederik Moechars, Matthew C Weston, Sandra Leo, Zsuzsanna Callaerts-Vegh, Ilse Goris, Guy Danels, A Buist, M Cik, Peter van der Spek, Stefan Kass, et al. Vesicular glutamate transporter VGLUT2 expression levels control quantal size and neuropathic pain. *Journal of Neuroscience*, 26(46):12055–12066, 2006.

[25] Lambda Moses and Lior Pachter. Museum of spatial transcriptomics. *Nature methods*, 19(5):534–546, 2022.

[26] Charlie Nash, Jacob Menick, Sander Dieleman, and Peter Battaglia. Generating images with sparse representations. In *International Conference on Machine Learning*, pages 7958–7968. PMLR, 2021.

[27] Eric Nguyen, Michael Poli, Matthew G Durrant, Brian Kang, Dhruva Katrekar, David B Li, Liam J Bartie, Armin W Thomas, Samuel H King, Garyk Bixi, et al. Sequence modeling and design from molecular to genome scale with Evo. *Science*, 386(6723):eado9336, 2024.

[28] Yaniv Nikankin, Niv Haim, and Michal Irani. SinFusion: Training Diffusion Models on a Single Image or Video. In *International Conference on Machine Learning*, pages 26199–26214. PMLR, 2023.

[29] Marius Pachitariu and Carsen Stringer. Cellpose 2.0: how to train your own model. *Nature methods*, 19(12):1634–1641, 2022.

[30] William Peebles and Saining Xie. Scalable diffusion models with transformers. In *Proceedings of the IEEE/CVF International Conference on Computer Vision*, pages 4195–4205, 2023.

[31] Adam Polyak, Amit Zohar, Andrew Brown, Andros Tjandra, Animesh Sinha, Ann Lee, Apoorv Vyas, Bowen Shi, Chih-Yao Ma, Ching-Yao Chuang, et al. Movie Gen: A cast of media foundation models. *arXiv preprint arXiv:2410.13720*, 2024.

[32] Robin Rombach, Andreas Blattmann, Dominik Lorenz, Patrick Esser, and Björn Ommer. High-resolution image synthesis with latent diffusion models. In *Proceedings of the IEEE/CVF conference on computer vision and pattern recognition*, pages 10684–10695, 2022.

[33] Urmas Roostalu, Casper BG Salinas, Ditte D Thorbek, Jacob L Skytte, Katrine Fabricius, Pernille Barkholt, Linu M John, Vanessa Isabell Jurtz, Lotte Bjerre Knudsen, Jacob Jelsing, et al. Quantitative whole-brain 3D imaging of tyrosine hydroxylase-labeled neuron architecture in the mouse MPTP model of Parkinson’s disease. *Disease models & mechanisms*, 12(11):dmm042200, 2019.

[34] Eduardo Sánchez-Mendoza, Marfa C Burguete, María Castelló-Ruiz, María Pilar González, Cesáreo Roncero, Juan B Salom, Carmen Arce, Sixta Cañadas, Germán Torregrosa, Enrique Alborch, et al. Transient focal cerebral ischemia significantly alters not only EAATs but also VGLUTs expression in rats: relevance of changes in reactive astroglia. *Journal of Neurochemistry*, 113(5):1343–1355, 2010.

[35] Hailing Shi, Yichun He, Yiming Zhou, Jiahao Huang, Kamal Maher, Brandon Wang, Zefang Tang, Shuchen Luo, Peng Tan, Morgan Wu, et al. Spatial atlas of the mouse central nervous system at molecular resolution. *Nature*, 622(7983):552–561, 2023.

[36] Jiaming Song, Chenlin Meng, and Stefano Ermon. Denoising Diffusion Implicit Models. In *International Conference on Learning Representations*, 2021.

[37] Christina V Theodoris, Ling Xiao, Anant Chopra, Mark D Chaffin, Zeina R Al Sayed, Matthew C Hill, Helene Mantineo, Elizabeth M Brydon, Zexian Zeng, X Shirley Liu, et al. Transfer learning enables predictions in network biology. *Nature*, 618(7965):616–624, 2023.

- [38] Robert J Vandenberg and Renae M Ryan. Mechanisms of glutamate transport. *Physiological reviews*, 93(4):1621–1657, 2013.
- [39] Britta Velten and Oliver Stegle. Principles and challenges of modeling temporal and spatial omics data. *Nature Methods*, 20(10):1462–1474, 2023.
- [40] Åsa Wallén-Mackenzie, Hanna Wootz, and Hillevi Englund. Genetic inactivation of the vesicular glutamate transporter 2 (VGLUT2) in the mouse: what have we learnt about functional glutamatergic neurotransmission? *Upsala journal of medical sciences*, 115(1):11–20, 2010.
- [41] Sonja M Wojcik, Jeong-Seop Rhee, Etienne Herzog, Albrecht Sigler, Reinhard Jahn, Shigeo Takamori, Nils Brose, and Christian Rosenmund. An essential role for vesicular glutamate transporter 1 (VGLUT1) in postnatal development and control of quantal size. *Proceedings of the National Academy of Sciences*, 101(18):7158–7163, 2004.
- [42] Jiqing Wu, Ingrid Berg, and Viktor Koelzer. IST-editing: Infinite spatial transcriptomic editing in a generated gigapixel mouse pup. In *Medical Imaging with Deep Learning*, 2024.
- [43] Jiqing Wu and Viktor H Koelzer. GILEA: In silico phenotype profiling and editing using GAN inversion. *Computers in Biology and Medicine*, 179:108825, 2024.
- [44] Jiqing Wu and Viktor H Koelzer. SST-editing: in silico spatial transcriptomic editing at single-cell resolution. *Bioinformatics*, 40(3):btae077, 2024.
- [45] Jiqing Wu and Viktor H Koelzer. Towards generative digital twins in biomedical research. *Computational and Structural Biotechnology Journal*, 2024.
- [46] Rui Xu, Xintao Wang, Kai Chen, Bolei Zhou, and Chen Change Loy. Positional Encoding as Spatial Inductive Bias in GANs. In *Proceedings of the IEEE/CVF Conference on Computer Vision and Pattern Recognition*, pages 13569–13578, 2021.
- [47] Zizhen Yao, Cindy TJ van Velthoven, Michael Kunst, Meng Zhang, Delissa McMillen, Changkyu Lee, Won Jung, Jeff Goldy, Aliya Abdelhak, Matthew Aitken, et al. A high-resolution transcriptomic and spatial atlas of cell types in the whole mouse brain. *Nature*, 624(7991):317–332, 2023.
- [48] Ailing Zeng, Yuhang Yang, Weidong Chen, and Wei Liu. The Dawn of Video Generation: Preliminary Explorations with SORA-like Models. *arXiv preprint arXiv:2410.05227*, 2024.
- [49] Meng Zhang, Xingjie Pan, Won Jung, Aaron R Halpern, Stephen W Eichhorn, Zhiyun Lei, Limor Cohen, Kimberly A Smith, Bosiljka Tasic, Zizhen Yao, et al. Molecularly defined and spatially resolved cell atlas of the whole mouse brain. *Nature*, 624(7991):343–354, 2023.
- [50] Zangwei Zheng, Xiangyu Peng, Tianji Yang, Chenhui Shen, Shenggui Li, Hongxin Liu, Yukun Zhou, Tianyi Li, and Yang You. Open-sora: Democratizing efficient video production for all. *arXiv preprint arXiv:2412.20404*, 2024.

Appendix

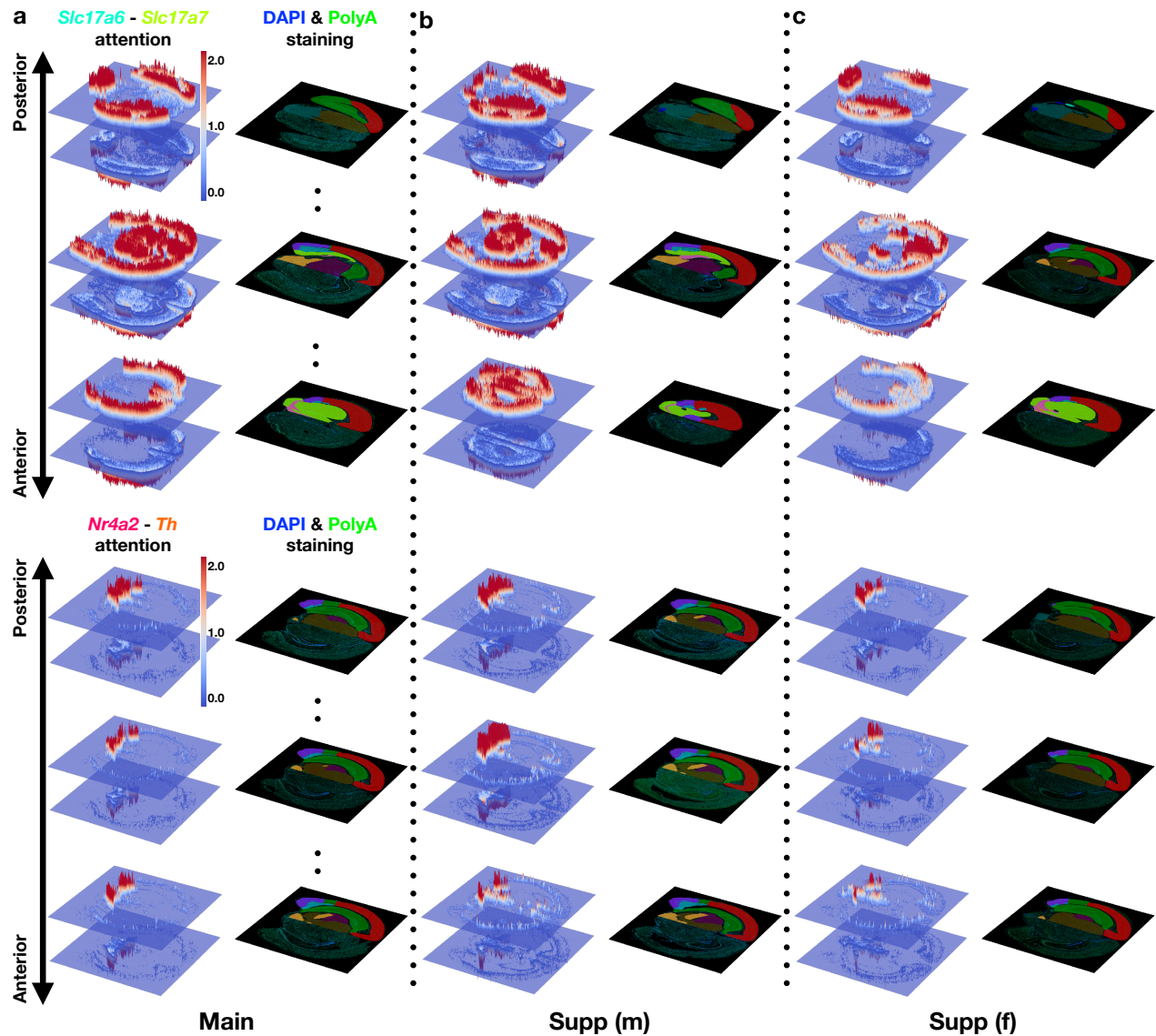


Figure 7: **The gene-gene interaction visualization of the previous-current and current-next slices along posterior to anterior direction for main and supp mouse brains.** **a.** The slice-wise visualization of *Slc17a6* and *Slc17a7* attention level (left) with regard to the DAPI- and PolyT-stained WSIs. **b.** The slice-wise visualization of *Nr4a2* and *Th* attention level (left) with regard to the DAPI- and PolyT-stained WSIs.

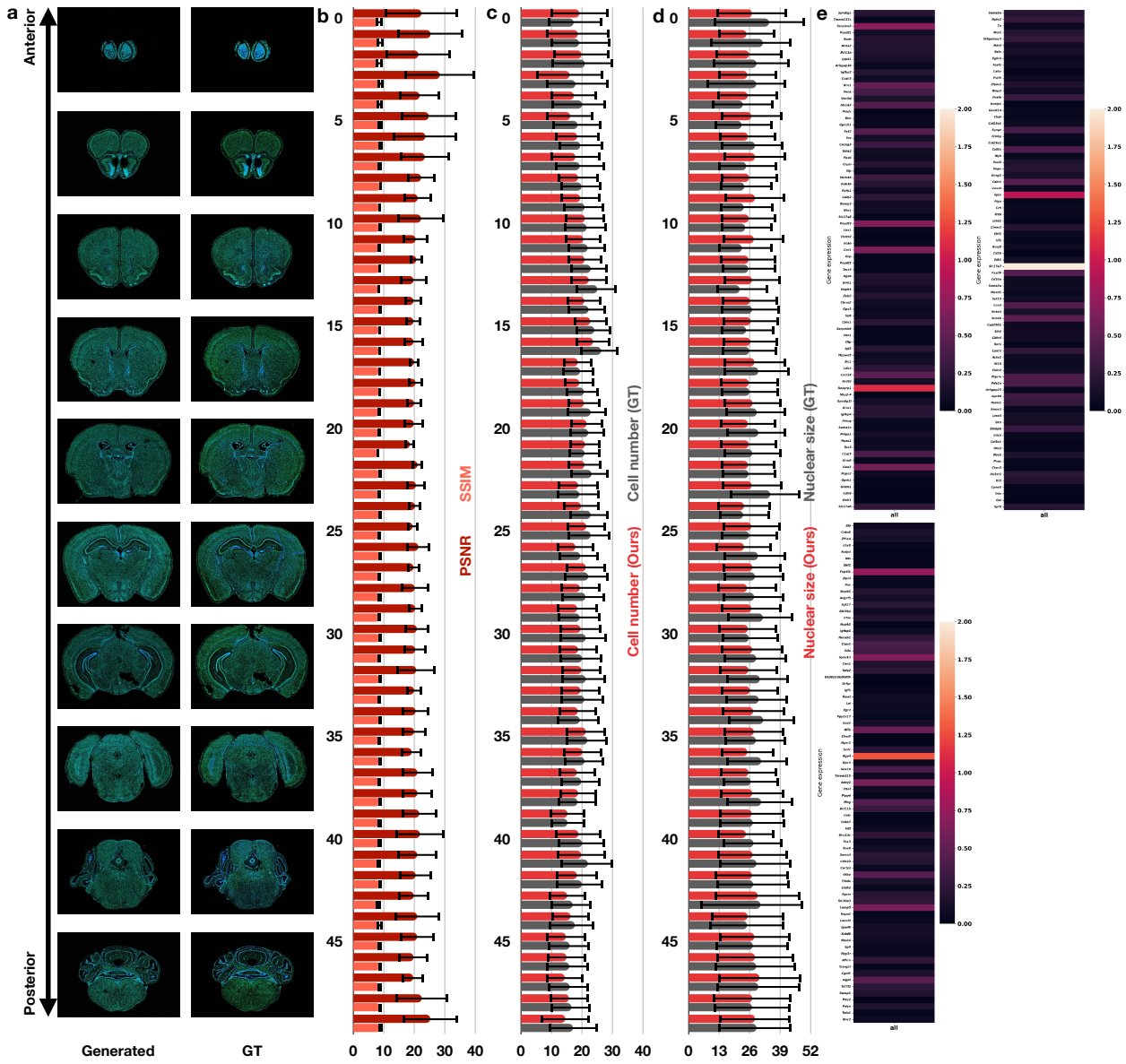


Figure 8: The comprehensive generation, quantification, and gene expression statistics for the mouse brain reported as the Main result. **a.** The side-by-side comparison between generated and GT WSIs. Here, we report the first of five consecutive slices for the sake of a clear visualization. **a.** For all the slices, we report the average PSNR and SSIM scores with standard deviation (std). **c.** For all the slices, we report the average cell number with std between our generated results and GT. **d.** For all the slices, we report the average nuclear size with std between our generated results and GT. **e.** The heatmap of overall 229-plex gene expression values normalized by log2.

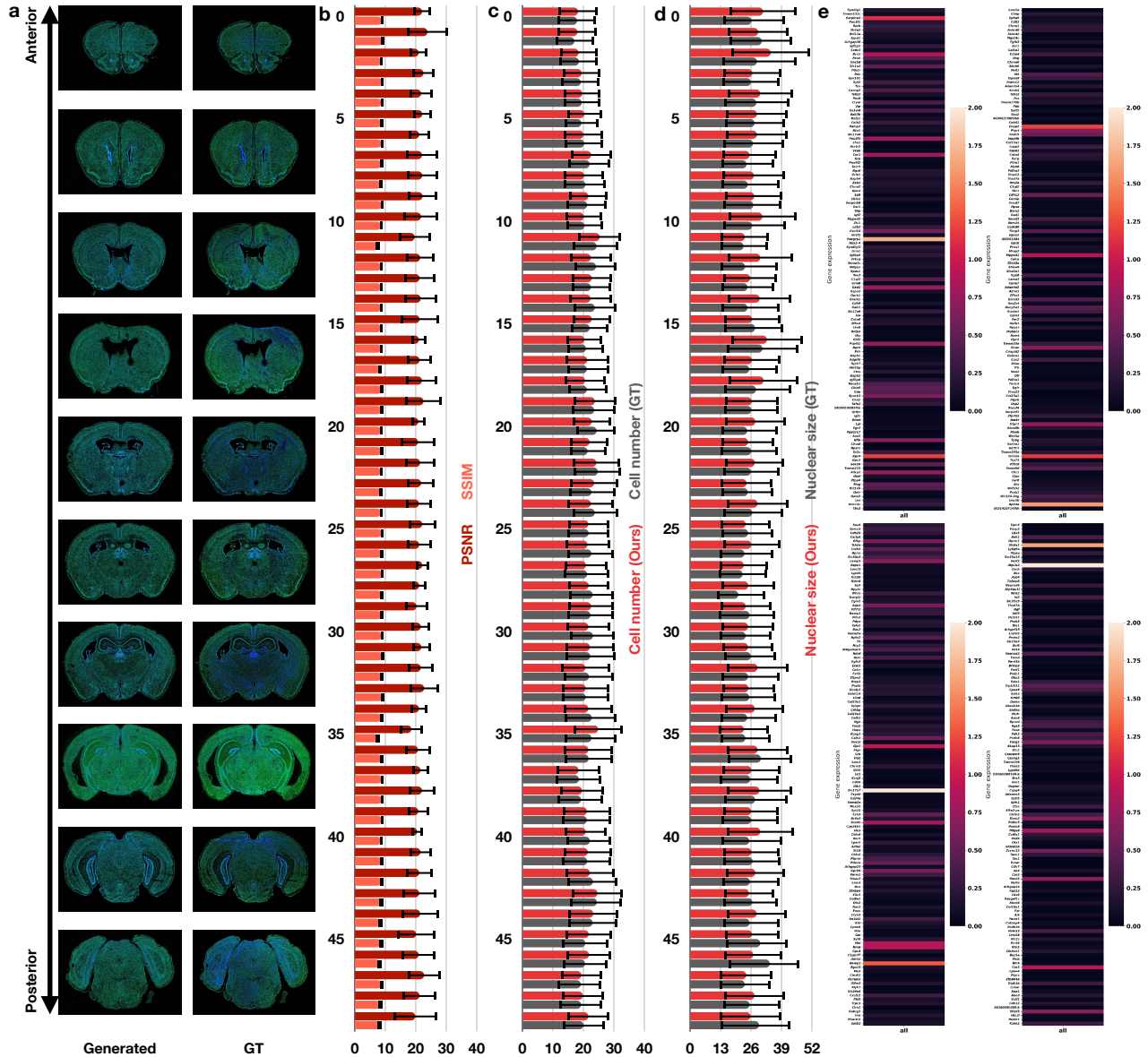


Figure 9: The comprehensive generation, quantification, and gene expression statistics for the mouse brain reported as the Supp (m) result. **a.** The side-by-side comparison between generated and GT WSIs. Here, we report the first of five consecutive slices for the sake of a clear visualization. **a.** For all the slices, we report the average PSNR and SSIM scores with standard deviation (std). **c.** For all the slices, we report the average cell number with std between our generated results and GT. **d.** For all the slices, we report the average nuclear size with std between our generated results and GT. **e.** The heatmap of overall 500-plex gene expression values normalized by log2.

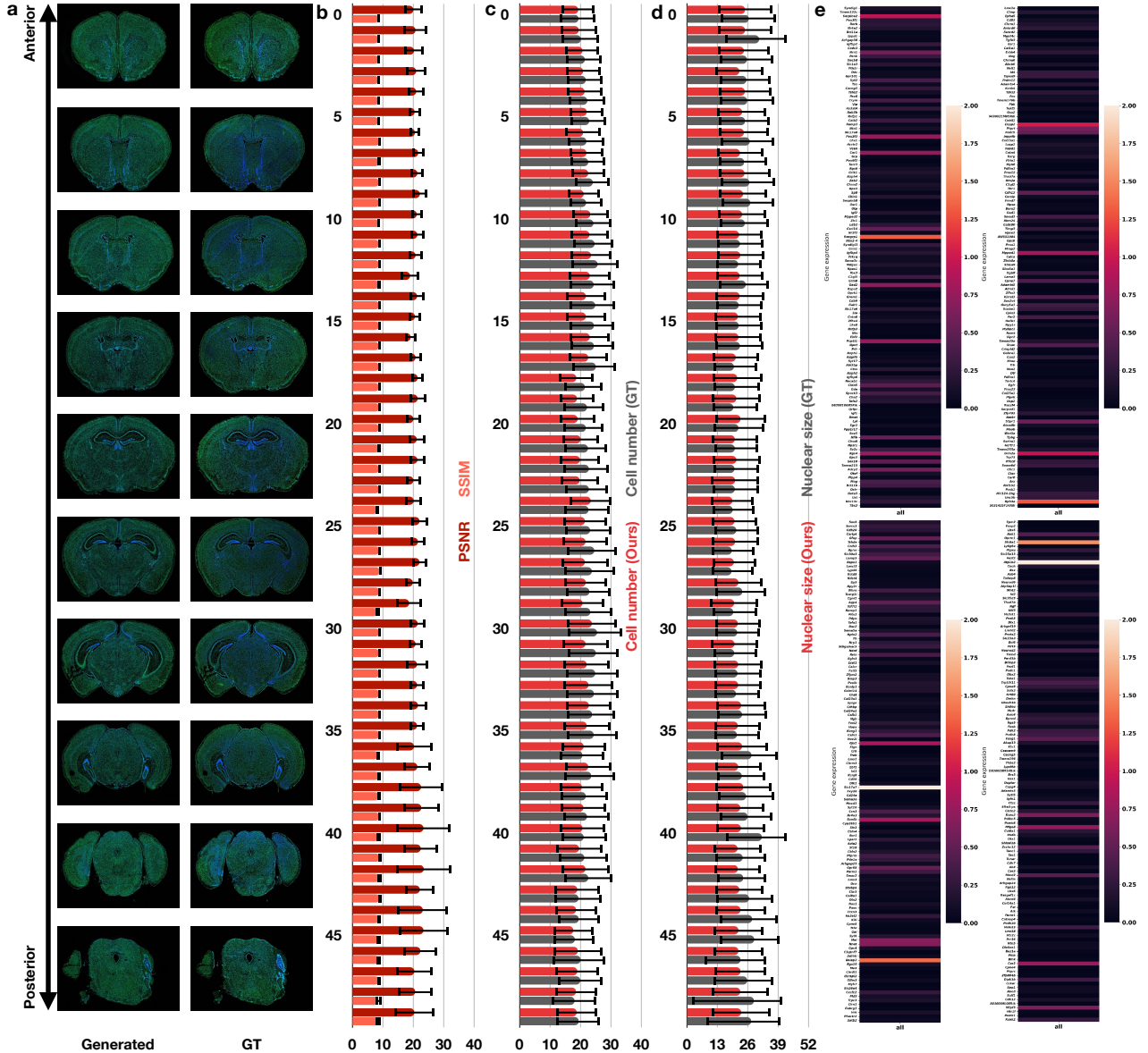


Figure 10: The comprehensive generation, quantification, and gene expression statistics for the mouse brain reported as the Supp (f) result. a. The side-by-side comparison between generated and GT WSIs. Here, we report the first of five consecutive slices for the sake of a clear visualization. a. For all the slices, we report the average PSNR and SSIM scores with standard deviation (std). c. For all the slices, we report the average cell number with std between our generated results and GT. d. For all the slices, we report the average nuclear size with std between our generated results and GT. e. The heatmap of overall 500-plex gene expression values normalized by log2.